Università degli Studi di Padova
Dipartimento di Fisica ed Astronomia "Galileo Galilei"

Corso di Laurea in Fisica

Characterization of the RF plasma in negative ion source NIO1

Relatore: prof. Gianluigi Serianni
Correlatore: Pierluigi Veltri

Laureando: Laura Buonincontri

Anno Accademico 2016/2017

Contents

Introduction

The NIO1 experiment is a negative ion source built at Consorzio RFX, Padua, with the aim to investigate and optimize the negative ion production towards the future requests for efficient methods to heat plasma inside the ITER prototype fusion reactor, that is under construction in France. With this purpose, a diagnostic of the plasma in the NIO1 source is essential. In this thesis a study of the NIO1 plasma was performed, focusing on the characteristics of the plasma in the region of the source located between the driver, where particles are created, and the extraction region, where ions are extracted and accelerated. The energy and density of the electrons in such region are very important to determine the performance of the source in terms of extracted negative ion current. The study presented here was made with experimental and numerical approaches. The measurements of the plasma were made by using an electrostatic probe inserted axially along the chamber, while the numerical simulation are based on the adaption of an existing code to reproduce the condition of the NIO1 source. This thesis is organized as follows. In the first chapter some generic characteristics of the ion source are presented, focusing on the NIO1 structure and operation conditions. Negative ions are created inside the plasma and have to be extracted from the source. In this chapter also why the electrons temperature inside the source plays a foundamental role will be explained. In the second chapter an overview of the diagnostic based on the use of a mobile Langmuir probe is reported. The main aspects of the theory of the Langmuir probes are firstly briefly summarized. By acquiring measurements of the current upon biasing this probe, some properties of the plasma can then be deduced. This device allowed the study of plasma parameters from the region in which plasma was generated to the extraction region.

In the third chapter the methods and choices applied to data analysis and results of the measurements are discussed. The conditions of the magnetic field, pressure and RF power coupling inside the source was changed during the campaign of measurements. Correspondingly a particular attention was paid to the study of the variation of electron temperature and density.

After that, in the fourth chapter,a numerical code already existent and used to study the behavior of plasma in presence of a magnetic field is adopted to model the NIO1 source. The choices made to adapt it and to reproduce some of the conditions created during the measurement campaign in NIO1 are described. The main aspects issued from the comparisons of simulation with experimental results are then shown.

Chapter 1

Ion Sources

The ion source devices are used in a rather wide variety of scientific and industrial fields.
The ion production, for example, is at the base of particle generation in high energy accelerators, ion implantation for semiconductor manufacturing, devices with medical scope, such as charged-particle accelerators for radiotherapy or for radionuclide imaging with positron emission tomography, and devices for fusion scope, such as the neutral beam injectors (NBI) for heating and fueling plasma inside fusion reactors[1]. In particular, the ion source studied in this thesis was built for the latter scope. The ion temperature required for achieving fusion reaction is about 10 keV. As the plasma resistivity decreases with increasing temperature, ohmic heating is limited to a certain temperature. A further heating of plasma to fusion temperatures of tens of keV is possible by injecting high energy neutral particle beams across magnetic fields. Neutral particles, obtained by a previous electrostatic ion acceleration and a successive neutralization [1], can enter the plasma confinement magnetic field and are ionised in the plasma via collisions with ions and electrons and transfer their kinetic energy to the plasma increasing its thermal energy. Such generated fast ions are also confined in the magnetic field and are able to exchange their energy to plasma ions and electrons. For instance, in fusion experiments such as ITER [1], still in costruction, which will be the world's largest magnetic confinement plasma physics experiment, neutral beams with energy up to 1MeV will be necessary.

A generic example of a ion source can be seen in Figure 1.1 (a): the two main parts are

- the plasma chamber, in which ions are produced in a confined. Inside the chamber an AC or DC discharge takes place and the neutral gas is ionized by coupling power to the gas with suitable power supplies. In the case of AC discharges the power can be coupled inductively or capacitively.[8] The plasma confinement, instead, occurs by means of permanent magnets disposed all around the source walls.

- the extraction area, in which ions are extracted and, outside the ion source biased electrodes form particle beams and accelerate them.

For fusion plasma heating, hydrogen or deuterium ions are usually used. Both accelerated positive or negative hydrogen ions can be used to produce energetic neutral beams. However, the choice of negative ions at high energies is compulsory: the neutralization efficiency of positive ions decreases as the beam energy increases, becoming unacceptably low at energies above 100 keV/nucleon. while negative ions have a neutralization efficiency around 60% even with the beam energies up to 1MeV. [6] Negative ions can be produced inside the plasma by volume or surface production. The volume production consists of a two step process: first the vibrational excitation of H_2 during collision with high energy electrons, then the excited molecule has a higher probability with respect to the ground state H_2 to capture an electron. The resulting H_2^- is unstable and dissociates into H_0 and H^-.
Fast atoms H_0 or ions H^+ are also converted in H^- ions, when colliding on the source walls (surface production). It was shown that injection of caesium vapor in the source leads to a 3-10 times enhancement in H^- surface production[**?**]. An important difference between postive and negative ions is that negative ions can be easly destroyed by collisions with high energy electrons. For this reason an electron cooling system is necessary in the extraction region.

Once generated in the volume of the source and in the surface of the extractor grid exposed to the plasma, negative ions closer to the extraction area can extracted and accelerated by the high electric field imposed by the biasing of electrodes in the accelerator.

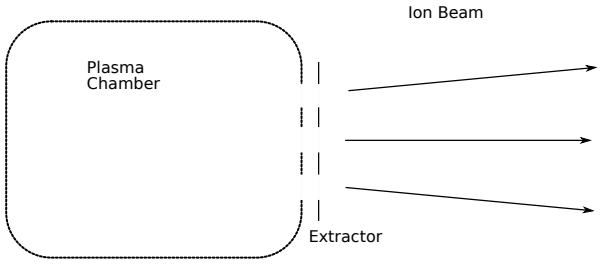

Figure 1.1: Schematic view of the ion source

1.1 NIO1 Experiment

NIO1 was designed and it is operated by Consorzio RFX and INFN in the framework of the accompanying activities for the development of Neutral Beam Injectors.

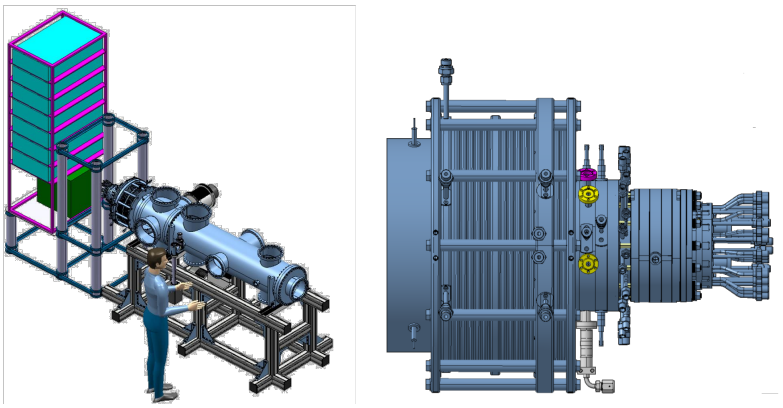

(a) Experimental setup of the NIO1 experiment (b) Source and extraction region overview

Figure 1.2

In Figure 1.2(a) there is an overview of the experiment. NIO1 is a negative ion source, based on the production of inductively coupled plasma with a radiofrequency (RF) system.

The three main components of the experiment are:

- Plasma Source

  The source (Figure 1.2 (b) and Figure 1.3) is composed by a cylinder having a radius of $5cm$ and a lenght of $21cm$. The driver, the region of

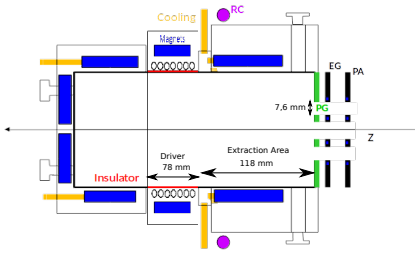

Figure 1.3: Scheme of NIO1 source

the source in which gas is ionized and plasma is generated, is placed almost at the centre of the chamber and extends for the lenght of $78mm$ and is surrounded by a 7 turns coil fed with alternate current at 2 MHz (radiofrequency)[7]. Here an azimuthal electric field is generated by the alternating magnetic field in the discharge region. If the imposed frequency is lower than the electron plasma frequency, electrons present in the gas volume can follow the oscillation of the RF electric field until they acquire enough kinetic energy to form a plasma by ionizing the background gas particles.

In the extraction region negative ions are extracted and pass through the 9 apertures of an electrode called Plasma Grid (PG), each aperture has a diameter of 7.6 mm, arranged in a 3x3 pattern.

There are three main sources of magnetic field in the NIO source with different aims: permanent magnets in multipole configuration with the aim of plasma confinement are disposed all around the chamber (Figure 1.4(a)), a transverse magnetic field with the aim of decreasing electron temperature is generated by a high current circuit in proximity of the PG, and other magnets are present inside the grids of the accelerator, in order to deflect coextracted electrons.

As said the electron cooling plays an important role in preserving the negative ions, because they are easily destroyed by energetic electrons.
The plasma cooling can be obtained by a transverse magnetic filter field, for reasons that will be better explained in the next section.

The Bias Plate (BP)[2], a pipe ($R = 5mm$) forming a rectangular frame around the extraction area, is placed 6.8mm before the PG.
The BP had been introduced in order to improve the amount of extracted negative ions and to reduce the co-extracted electrons; in NIO1, originally it also created the transverse magnetic field in proximity of the Plasma Grid,and had the function of returning the current flowing throught the PG. Then, to increase the magnetic field strength, a second configuration was adopted. In this new configuration the current flows through the PG, and returns through external conductors (Figure 1.4(b)). The resulting magnetic field profile, can be seen in 1.4(d).

Consequently in the present configuration the BP is an electrode which can be biased with rispect to the wall independently from the PG, and in this experiment has been used to influence the behavior of the plasma in the extraction area. The intensity of the magnetic field can be studying changing the values of the current driven both through the PG, which is electrically insulated from the source chamber, and the resulting magnetic field is directed along the vertical direction. The electrical connection between these components are presented in (Figure 1.4(e)). In the exper-

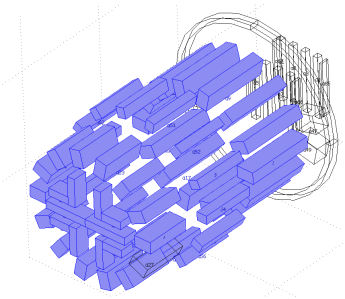

(a)

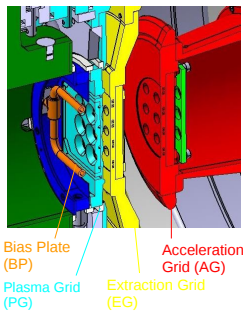

(b)

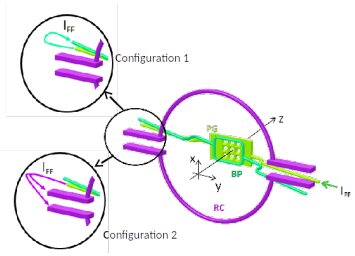

(c)

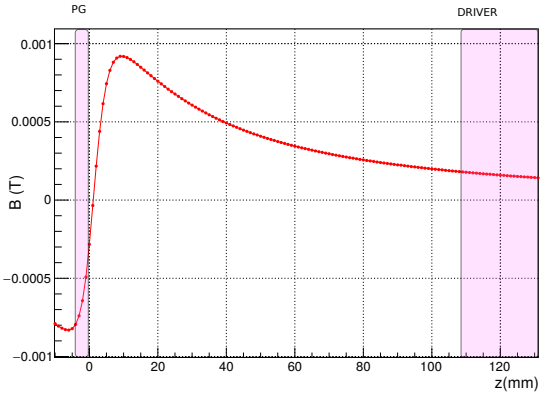

(d)

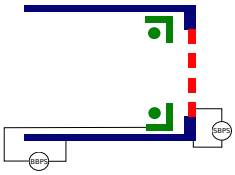

(e)

Figure 1.4

iment which is going to be presented, the current flowing in the PG can be varied in the range 0-400 A with a corresponding variation of the B profile.
Finally, the caesium vapor in order to improve the negative ion production has not been introducted yet. In the absence of caesium vapor, negative ions represent everywhere only a fraction of the negative charge.

- Acceleration column
  The extracted ions are then accelerated by passing through a series of polarized electrodes(Figure 1.4(b)). The NIO1 accelerator is composed by three grids: the plasma grid biased at $-60kV$, the extraction grid (EG) at -52kV and the post acceleration grid (PA) at a potential close to ground.

  NIO1 features 9 apertures, arranged in a 3x3 lattice. The central aperture is aligned with the source axis. During this diagnostic operation the acceleration column was not used, because this work was dedicated in studying the plasma inside the NIO1 source.

- The diagnostic Tube is $2m$ long cylindrical vessel, where the accelerated beam drifts towards a diagnostic calorimeter. Many flanges and viewports are installed on the vessel as access points for diagnostic devices.

1.1.1 Magnetic field and collisions

The main effect of magnetic field is the curvature of the ion and electron trajectories in the direction orthogonal to the field lines, while in the parallel direction, the motion of the particle is unperturbed. The radius of the orbit is the Larmor radius and can be calculated both for electrons and ions upon knowing their mass and temperature:

$$R_{Le} = \frac{\sqrt{2m_e k_B T_e}}{qB}$$

$$R_{Li} = \frac{\sqrt{2m_i k_B T_i}}{qB}$$

Generally the effect of the magnetic field is more evident on electrons, having a smaller gyration orbits with respect the ions at least by the factor $\sqrt{\frac{m_e}{m_i}}$, the ratio changes if T_i is not comparable to T_e.

The presence of magnetic field changes the diffusion coefficients inside the plasma, which becomes anisotropic.
When an electron gyrating around a line of force suffers a collision, it changes its direction, and its center of gyration is displaced by a factor comparable with the Larmor radius.

Calling D_0 the ambipolar diffusion coefficient in the absence of magnetic field, k_B the Boltzmann constant ω_c the gyrofrequency and ν_c the collision

frequency we note that the diffusion coefficient in the direction parallel to the field line is simply:

$$D_{\parallel} = D_0$$

while, in the orthogonal direction:

$$D_{\perp} = D_0 \left(1 + \left(\frac{\omega_c}{\nu_c}\right)^2\right)^{-1}$$

$$D_0 = \frac{k_B T}{m \nu_c}$$

with

$$\nu_c = \frac{n e^4}{16 \pi \epsilon_0^2 \sqrt{m_e} (k_B T)^{3/2}}$$

From which, for $\frac{\omega_c}{\nu_c} >> 1$

$$D_{\perp} = \frac{k_B T \nu_c}{m \omega_c^2}$$

.

and by replacing the previous expression for ν_c:

$$D_{\perp} \propto \frac{1}{\sqrt{T}}$$

This means that more energetic particles have lower mobility in the direction perpendicular to the magnetic field lines[8].

A weakly ionized plasma as it is the case of NIO1 experiment, collision of electrons with neutral particles cannot be neglected. In particular for electronic temperature between 1-10eV the collision with neutral gas are dominant with respect to the collisions among plasma particles (Coulomb collisions). The collision frequency for electrons on neutral particles is proportional to the neutral gas density [9]. For this reason an increase of the neutral density implies an higher collision frequency and an electron energy loss.[9]

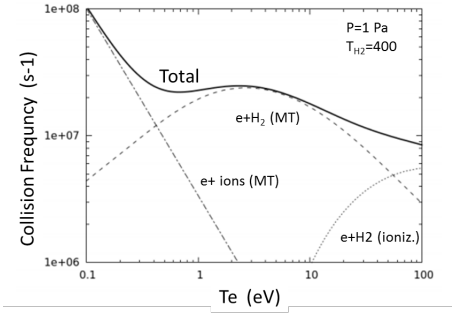

Figure 1.5: Collisions frequency as a function of Temperature

Chapter 2

Diagnostic Setup

The characteristics of the plasma inside the expansion region of the NIO1 source play a fundamental role in determining the amount of negative ions and electrons that are extracted trought the apertures placed at its end. In particular the plasma behaviour is influenced by several source parameters, such as the neutral gas pressure, the RF power, the intensity of the B field (generated by current flowing through the plasma grid and related conductors) and the bias of some electrodes inside the source. To investigate the plasma behaviour as a responce of variation in these parameters, a suitable diagnostic is required. In this section of the thesis the diagnostic setup used, constituted by an electrostatic probe is described.

2.1 Electrostatic Probes

The use of electrostatic probes is one of the most important techniques for measuring the properties of plasmas, studied by Langmuir since 1924. Experimentally, electrostatic probes are simple devices, which consist of a metallic electrode inserted into the plasma.
These electrodes can be biased by connecting them to a power supply and is it possible to deduce some plasma characteristics by measuring the collected currents.
Measurements made by means of Langmuir probes are local measures allowing to study of the dependence of the collected current as a function of the bias voltage applied to the electrode. in order to deduce the local plasma density, the electron temperature and the floating potential.
Since the mean ion speed is smaller than the mean electron speed, when an electrode electrically insulated is inserted in the plasma it would rapidly charge up negatively, and starts repelling more electrons and attracting ions, until a stationary condition is reached and the net electrical current goes to zero.[10]
Consequently, a positive layer forms at the interface between the plasma and the object surface, for the reason explained in the Electrostatic Probe section of

the previous Chapter 2.1. This layer is called the Debye sheat and its thickness is typically a few Debye lenghts wide.

The Debye Lenght, whose expression is:

$$\lambda_D = \sqrt{\frac{\epsilon_0 T_e}{q^2 n_e}} \tag{2.1}$$

is an important characteristic lenght in plasma: it is the distance scale over which significant charge densities can spontaneously exist. It is on space scales larger than a Debye length that the plasma will tend to remain neutral. [4] The potential reached by this floating probe is called floating potential (it will be denoted with V_f). If the potential of the probe is varied, the collected current by the probe also changes. A typical voltage–current characteristic for an electrostatic probe is shown in Figure 2.1. If the potential of the probe is kept at the same potential as the plasma V_P it will be mainly reached by electrons, so most of the drawn current will be due to electrons. Upon reducing $V < V_P$, electrons are repelled and ions are attracted, until at V_f the probe bias is sufficiently negative to equalize the flux of electrons repelled and ions attracted. By reducing V, for $V < V_f$ the flux of ions collected by the probe dominates, tending to the so-called ion saturation current (that may also vary with voltage if the effective collection area in not constant). By biasing the probe to a potential $V > V_P$, the current collected will be mostly electronic because all ions are repelled and in the case of planar probe and in absence of any magnetic field, it saturates to a current usually called electronic saturation current. The expressions of ion and electron saturation currents are[8]:

$$I_i(V) = -\frac{1}{2} e n_e A \sqrt{\frac{k_B T_e}{m_i}} \tag{2.2}$$

$$I_e(V) = \frac{1}{4} e n_e A \sqrt{\frac{8 k_B T_e}{\pi m_e}}$$

where n_e is the electron density, A is the probe area and T_e the electron temperature, m_i the ion mass and m_e the electron mass. In the transition region the current is given by

$$I(V) = I_i + I_e exp\left(\frac{e(V - V_p)}{k_B T_e}\right) \tag{2.3}$$

2.2 Probe support and motion system

A schematic of the probe set up inserted into NIO1 vessel is reported in Figure 2.2(a). Due to the reduced accessibility of the NIO1 source, and to the lack of an axial port on the source body, it has been decided to insert the probe into the plasma through the accelerator apertures. This implies that extraction and

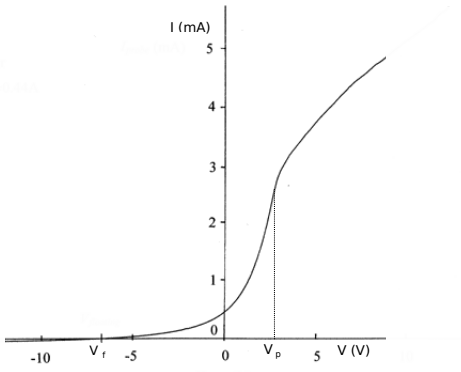

Figure 2.1: I-V probe characteristic

acceleration of negtive ions cannot take place during this experimental campaign. The source and the accelerator electrodes, in fact, were all connected to the same reference ground. In figure 2.2(b) a more detailed scheme of the probe support is presented. The probe tip assembly, consisting of a tungsten rod inserted into a thin quartz tube to insulate it from the plasma, was supported by a $2.6m$ long shaft with an outer diameter of $16mm$, which allowed the insertion of the probe all along the diagnostic chamber and into the central hole of the accelerator, in order to reach the source.
Using a lateral port of the diagnostic tube, it was possible to check the alignment of the probe tip with the central aperture of the grid. Using the external manipulator it was possible to regulate the insertion of the probe into the source. In this experiment the probe was inserted up to $10cm$ from the plasma grid, which is not the entire length of the source, in order to avoid alterations of the plasma; nonetheless it allowed to scan the entire width of the extraction area of the source.

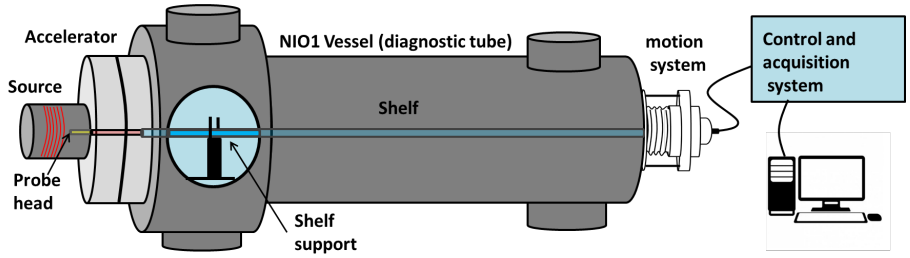

(a) Schematic view of the diagnostic setup

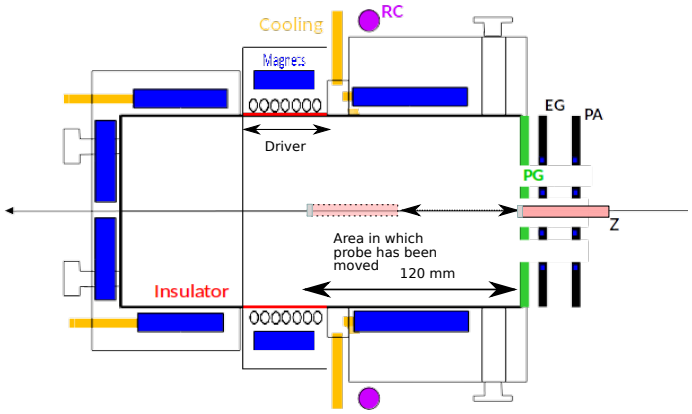

(b) Insertion of the probe into the chamber

Figure 2.2

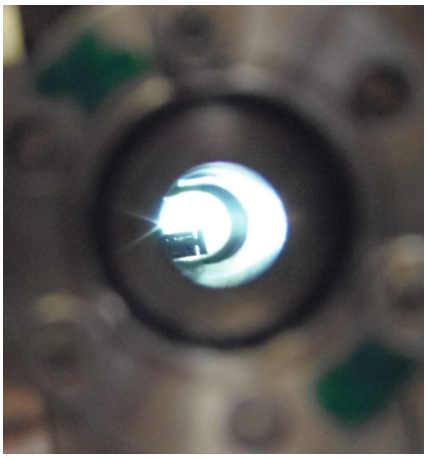

Figure 2.3: A view of the probe form the lateral viewport of the NIO1 source. The view port is placed at $z = 19mm$ from the PG, and has a diameter of $8mm$. It was used to verify the probe alignment and axial (z) position inside the source.

2.3 Probe connection and circuit

A scheme of the main components of the acquisition system is presented in Figure 2.4. The signal collected on the probe head is brought by a coaxial cable whose insulating parts are realized in a vacuum compatible material (kapton). The cable is then connected to a feedthrough at the end of the support shaft to transfer the signal from the vacuum to air condition. The metallic shield (external conductor of the kapton wire) and the rack of the acquisition system are connected to a screw fixed to the vessel, which is at the Earth potential.

The acquisition system is based on a Raspberry-PI, a single board small com-

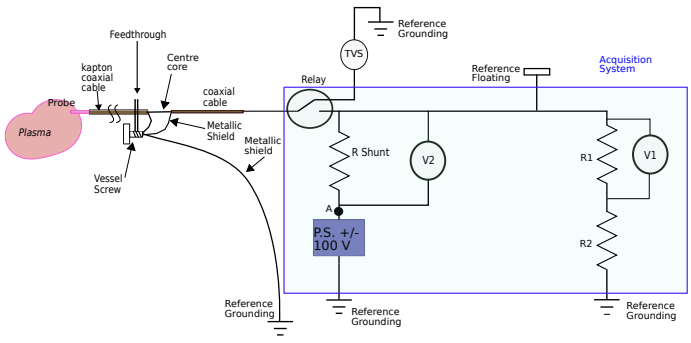

Figure 2.4: Probe circuit

puter provided with Linux operative system. The Raspberry can send and receive digital signals and an extension board was introduced and added to the Raspberry basic features, with analogue to digital converter (ADC) and digital to analogue converter (DAC) functions. The extension board is provided with an output 12 bit DAC channel and two input 12 bit ADC channels to convert signals.

The laboratory computer is connected to the Raspberry that drive the biasing of the probe and can be triggered remotely via a LAN network from a standard PC; from which it is possible to set the voltage output, writing the voltage in bit into a dedicated file which is stored into the Raspberry memory.

Using the ouput channel, it is possible to apply a voltage to the probe in the point A of Figure 2.4, thus polarizing the probe.

When the negative voltage is applied to point A, the probe starts collecting current. The output measures are the two voltages labeled as $V1$ and $V2$ in Figure 2.4. Using the resistor $Rshunt$ it is possible to obtain the current collected by the probe, while, using the resistor $R1$ of the voltage divider we can obtain the applyed voltage between the reference grounding and the probe head. This should be identical to the input voltage applied by the Raspberry.

The signal from $V1$ or $V2$ reaches the ADC channel. All these measures are written in a binary file which is stored into the Rasberry solid state memory. A relay has the function to bring the probe to the floating potential after measures has been done, in order to protect the probe from electron and ion fluxes for prolonged time since they could overheat the probe nead and cause damages.

2.4 Preliminary Tests

Some preliminary tests were performed to verify the conversion factor between voltage and bit in the absence of plasma and using two voltmeters. By comparing the current measured across the shunt and the divider, a small component of parasitic current was found and during the following analyses this component was subtracted from measures. In order to evaluate the acquired signal with a known component the circuit was modified and an Rtest was introduced as in figure 2.5(a) to simulate the resistance of plasma. The voltage applied to point A was varied from -80 to 80V, in order to test the entire range of expected voltage. Through an easy analysis of the dependence of current collected and stored in the Raspberry from the voltage applied, it was possible to conclude that values of resistance obtained from these tests corresponded to the known value of the Rtest: 2.5(b) presents an example of the obtained scan. The inverse value of the slope of the (V,I) recorded curve, in fact, is compatible with the selected value of the test resistance.

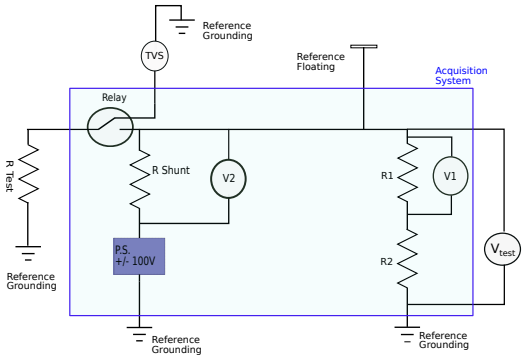

(a)

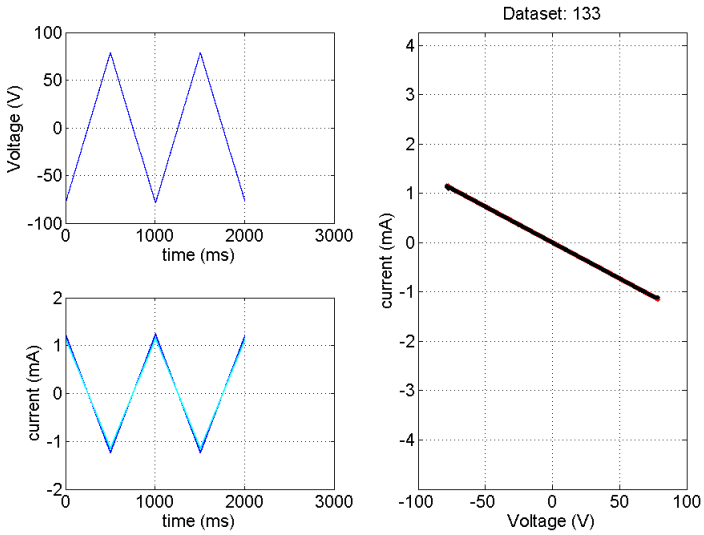

(b)

Figure 2.5: Preliminary tests

2.5 Changing of parameters during the measure

The characteristic I-V of the probe was acquired at different distances from the plasma grid, by applying to the probe a variable voltage from -80V to -10/10V. The voltage to collect the ion current, in fact, was limited to few Volts, to avoid high power fluxes to the probe, so the electronic side of the characteristic was not reached. Anyway, for the kind of model used to analize data (that will be exposed in the next chapter), it is not necessary to reach the electron saturation current to estimate the electron density and temperature and the floating potential. The value of the voltage was tuned from time to time depending on the RF power and probe position, to avoid large current in the case of high plasma density. In any case the voltages were sufficient to evaluate the plasma density and temperature by fitting the collected data.

Chapter 3

Data Analysis

3.1 Fit Formula

If the sheath thickness is small compared to the probe radius, it is possible approximate the collection area A in formula 2.3 with the surface area of the probe, and the ion current would theoretically result independent from the probe potential[10]. In practice, a further increasing of the ion current collected as the probe potential becomes more negative is noticed.
This non saturation of the ion current can be explained as a consequence of the fact that the sheath thickness increases as the probe potential is made more negative, and the collecting area of the probe increases as well. This aspect has already been studied and an alternative expression for the ion saturation current was found [11].

$$f = -e^{a}\frac{q}{2}\sqrt{b\frac{q}{m_i}}A[1 + c(d - x)]\left[1 - e^{\frac{x-d}{b}}\right] \tag{3.1}$$

This expression is the fitting formula used to fit data collected by the electrostatic probe and is valid for voltage value until about the floating potential. Here the four fit parameters (a,b,c,d) are related with the plasma parameters as follows: $a = log(n_e)$,with n_e being the electron density, $b = T_e$, electron temperature, c is the parameter which contains the variation of the probe area, $d = V_f$ is the floating potential.

This formula has been used directly on the raw data. In figure3.1(a) and 3.1(b) a typical sample of data acquired with the probe and an example of data fitting using the formula 3.1 are presented: it can be noticed that as only the first part of the curve has been fitted, to respect the validity range of the formula. Data analysis was performed in the Root environment.

The stimated parameters for this fit are:

$$a = 39.1808 \pm 0.0005$$

$$b = 7.01 \pm 0.01$$

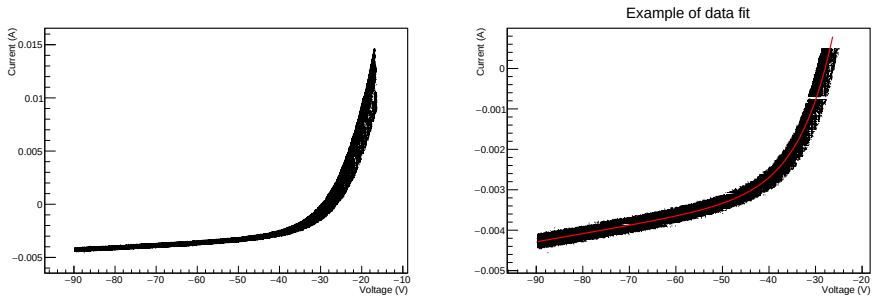

(a) Example of acquired characteristic (b) Example of data fitting

Figure 3.1: Example of a typical acquired characteristic

$$c = 0.00660 \pm 0.00002$$
$$d = -27.948 \pm 0.004$$

3.2 Propagation of data variances to the fit parameters

The errors obtained directly from non linear minimization resulted too small to be credible: we can see also in Figure 3.1 that the deviation of data from the fitting curve is not small even if they are well fitted by the curve.
The fluctuation associated to T_e and n_e can be assumed to be Gaussian distributed, but they are non-linearly propagated to the probe current, as they compare in the exponential in the fit formula.
To give a realistic error to these parameters I follow this procedure (see 3.2): for each set of data (I,V characteristic) an interval in the x axis was selected, in proximity of the lower value of the voltage, and the standard deviation (σ_y) of data, from the mean value of the corresponding data in the y axis, was calculated. This deviation was used as an estimate of the error on the current. Similarly, an interval in current was selected in the exponential part of the curve, for values of current not too high, because for higher values the exponential trend is no longer respected. The deviation σ_x from the mean value of the voltage in that interval was calculated and used as an estimate of the error on the data in voltage and electron temperature.

In order to find the error on n_e the formula for the ion saturation was used and the error on n_e was calculated by the error propagation formula.

$$I = -n\frac{q}{2}\sqrt{\frac{T_e q}{m}}A$$
$$n = -\frac{I}{\frac{q}{2}\sqrt{\frac{T_e q}{m}}A}$$

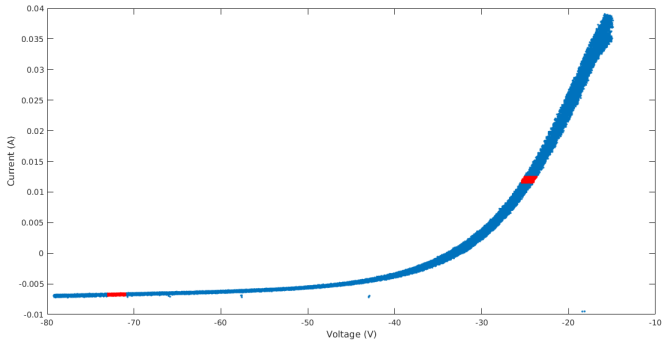

Figure 3.2: In red, intervals in current and voltage

$$\frac{\sigma_n}{n} = \sqrt{\left(\frac{\delta n}{\delta Te} \cdot \sigma x\right)^2 + \left(\frac{\delta n}{\delta I} \cdot \sigma y\right)^2}$$

$$\frac{\sigma_n}{n} = \sqrt{\left(\frac{\sigma_y}{I}\right)^2 + \left(\frac{\sigma_x}{T_e \cdot 2}\right)^2}$$

3.3 Scan in probe position

The probe was inserted into the source,and for each position the probe current-voltage characteristic was constructed. Upon varying the external condition such as the pressure, the RF power and the intensity of the magnetic field, it was possible to study how plasma parameters change. The configuration of the magnetic field used in this experiment is the one explained in Chapter 1. The plasma inside the chamber was studied:

- by varying the probe position while fixing the external condition such as the magnetic field in the extraction area, the pressure of the neutral gas, the RF power
- by keeping fixed the probe position while varying the external condition.

Some preliminary remarks have to be made for all scans in position: in order to ass the effect of the probe on the plasma, it is reported here the PG bias (BBPS) and the BP bias (SBPS), at different positions of the probe. These graphs show that there is a variation on the current collected by the power supplies that are biasing the PG the BP with respect to the walls. These variations can only be due to the changing of plasma potential, because the current flowing through the PG and the potential at which the BP has been set were fixed during the scan. Points near the PG (from $z = 0mm$ and $z = 10mm$) and points next to

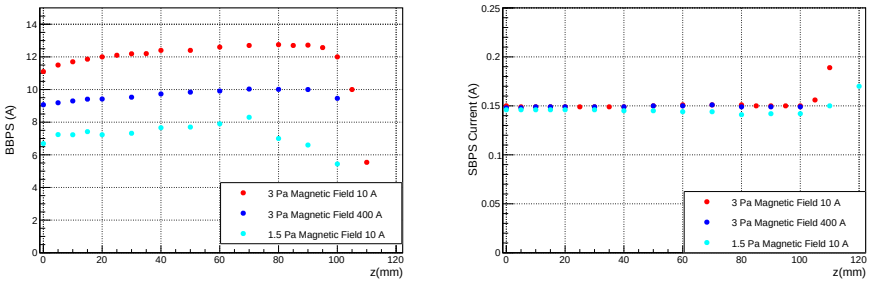

(a) BPPS along z, magnetic filter at 10 and 400 A

(b) SBPS along z, magnetic filter at 10 and 400 A

the driver have not been considered because:

- near the PG, particle motion is strongly influenced by the magnetic field due to the permanent magnets inside the EG, and particles are then deflected by the magnetic field until they hit the PG.

- When the probe reached the driver, indeed, the plasma was strongly perturbated. During the experiment this was evident because of the suddently changing of the Bias Plate and the Plasma Grid polarization which attest a perturbation of the plasma.

In the following sections some of the results of the data analysis are presented. All the other scan analized can be found in the Appendix 5.

3.3.1 Magnetic Filter

For each scan that will be presented in this and in the next sections, all the operation conditions set are summarized in a table.
As it was explained in 1.1 the magnetic filter value could be set by changing the flowing current trought the PG and the external conductors, that can be varied in the range 10-400 A.

The typical profile of magnetic filter was presented in 1.4(d).
The first data presented constitute a scan of the position,with the magnetic filter current values fixed at its minimum and maximum value. Then, while keeping the probe position fixed at 20 and 90 mm, the magnetic filter was varied. In order to investigate the effects of the magnetic filter on plasma parameters, two scan in position was made: the first by setting the magnetic filter at its lower value and the second by setting it at its maximum value. Then, while keeping the probe position fixed at 20mm and 90 mm, the magnetic filter intensity was varied.

Plasma conditions

RF Power	Pressure (Pa)	Magnetic Filter (A)	Bias Plate Current (A)
1000	3	10	0.01
1000	3	400	0.01

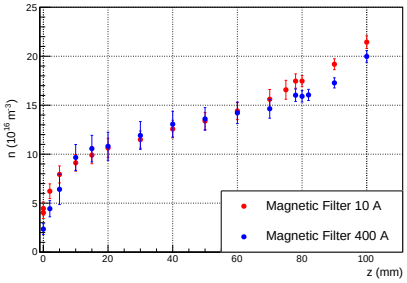

(a) n along z, magnetic filter at 10 and 400 A, gas pressure 3Pa

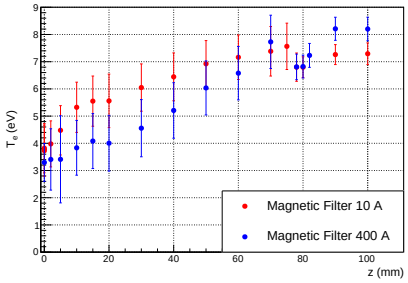

(b) T_e along z, magnetic filter at 10 and 400 A, gas pressure 3Pa

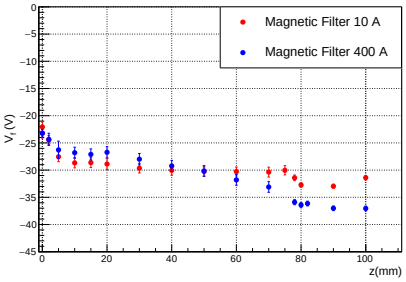

(c) V_f along z, magnetic filter at 10 and 400 A, gas pressure 3Pa

As expected, as the probe is inserted deeper in the chamber, the density and the temperature increase, but have different slope for low or high magnetic field.

The first evidence is that the electron temperature for low magnetic field is in general higher with respect to the other, in particular between $10mm$ and $20mm$. This is what was expected, because in these positions the effect of the magnetic field is stronger.

On the other hand, the magnetic confinement of hot electrons is not evident: the electron density is expected to be lower in areas where magnetic field is stronger and higher elsewhere, while between $z = 60mm$ an $z = 100mm$ this is not verified. Maybe this could be explained by the fact that even if the magnetic field is strong enough to reduce the electron temperature, its strength is not sufficient to influence heavily the electron distribution function.

Plasma conditions

RF Power	Pressure (Pa)	Position (mm)	Bias Plate Current (A)
900	3	20	0.01
900	3	90	0.01

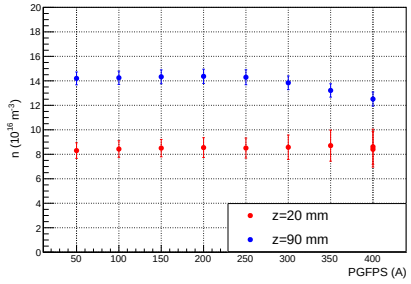

(a) n at fixed position $z = 20mm$ and $z = 90mm$ as a function of magnetic filter strength

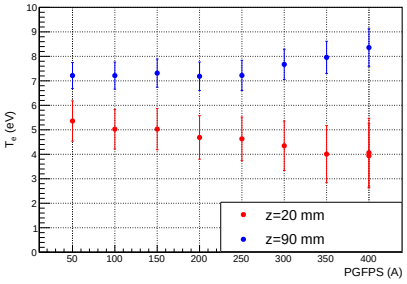

(b) T_e at fixed position $z = 20mm$ and $z = 90mm$ as a function of magnetic filter strength

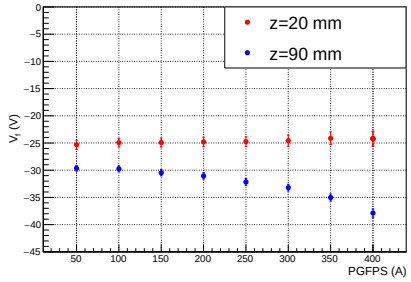

(c) V_f at fixed position $z = 20mm$ and $z = 90mm$ as a function of magnetic filter

Figure 3.3

The scan in 3.3 was performed with the probe at the fixed positions of $20mm$ and $90mm$. It is important to remember that the magnetic field is concentrated in the first 3-4 cm of the chamber, so its effect is expected to be more visible in the scan at 20mm. At 20 mm position , the temperature decreases as the magnetic filter becomes stronger, while the density remains constant. At position 90mm, instead, the temperature increases as the magnetic field becames stronger, while the density decreases. This seems to suggest that the magnetic filter confines the high energy particles, that are smaller in number.

Plasma conditions

RF Power	Pressure (Pa)	Magnetic Filter (A)	Bias Plate Current (A)
1100	6	10	0.01
1100	6	400	0.01

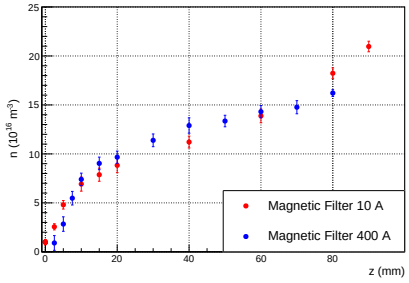

(a) n along z, magnetic filter at 10 and 400 A

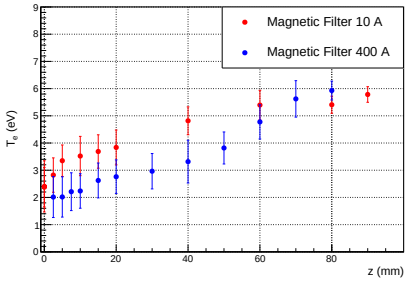

(b) T_e along z, magnetic filter at 10 and 400 A

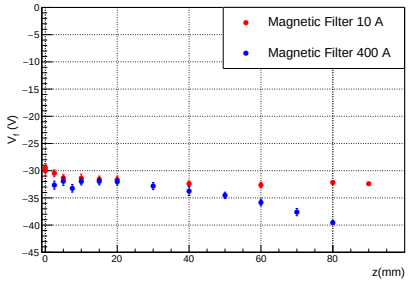

(c) V_f along z, magnetic filter at 10 and 400 A

Figure 3.4

In the scan at 6 Pa the qualitative behaviour is similar to the case at lower pressure, but the electron cooling due to the magnetic field in weaker than in the other analized cases because the higher pressure of the neutral gas has already made a cooling effect due to the higher electrons collision frequency with neutral gas, as exposed in the first chapter, section 1.1.1.

3.3.2 Pressure

The effect of pressure of the neutral gas on the plasma in NIO1 chamber was also investigated.

First, a scan with the probe fixed position and varying the pressure of the neutral gas was made:

Plasma conditions

RF Power	Position (z)	Filter Field (A)	Bias Plate (A)
1100	10	10	0.01

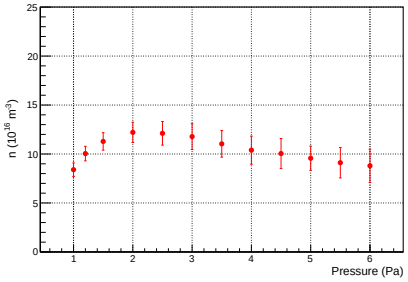

(a) Density at fixed position $z = 10mm$ with different values of pressure

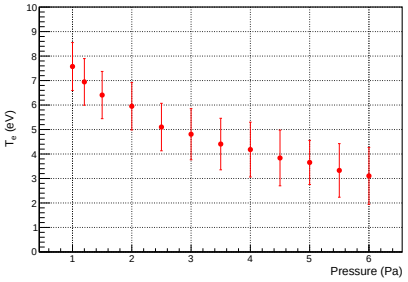

(b) Temperature at fixed position $z = 10mm$ with different values of pressure

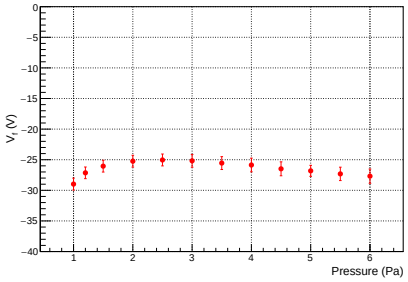

(c) Floating potential at fixed position $z = 10mm$ with different values of pressure

Figure 3.5

From this scan it can be observed that the electron density has a maximum for a value of pressure of 2 Pa, and it is possible to deduce that there is a maximum of ionization with respect to the pressure.
The effects of the pressure on the temperature are clear: the electron temperature decreases as the pressure increases. A similar result was obtained also in the theorical simulation of NIO plasma. [9]

Also some scan in position at different fixed pressure were performed:

Plasma conditions

RF Power (W)	Pressure (Pa)	Filter Field (A)	Bias Plate (A)
1100	1.5	10	0.01
1100	3	10	0.01
1100	6	10	0.01

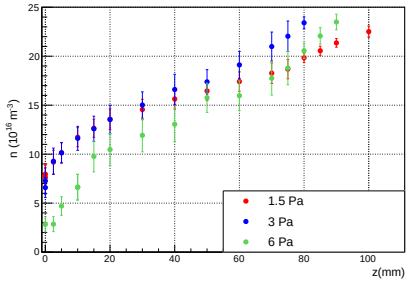

(a) Density along z with different values of pressure

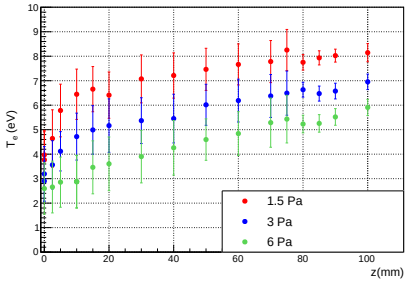

(b) Temperature along z with different values of pressure

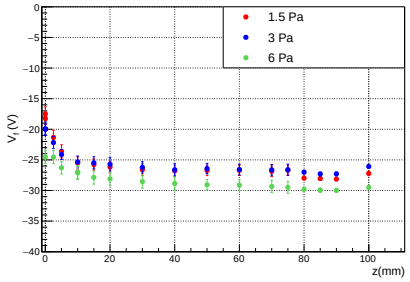

(c) Floating potential along z with different values of pressure

Figure 3.6

The presence of a maximum in electron density, as seen in the previous scan, can explain the fact that the density trend in the scan in position at a pressure of 3 Pa is not so different from that at the pressure of 1.5 Pa, but the difference with the case at 6 Pa is greater. Concerning the behaviour of the floating potential measured at the pressure of 6 Pa, it seems different from what was measured a lower values of the pressure.

This is confirmed by the voltage of the BP (which in this case it was leaved floating) has been taken from the database [17], as displayed in 3.7; This figure also shows that the disturbance induced by the probe insertion is not too large.

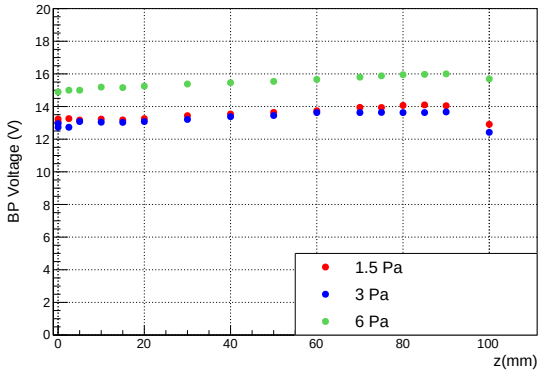

Figure 3.7: BP voltage as a function of a probe position, various pressures

3.3.3 RF Power

Also in the study of RF Power, a previous scan by varying the position of the probe was performed for different values of RF power. A linear dependence of density with respect to the RF Power can be expected from numerical simulations [9] [20].

Plasma conditions

RF Power (W)	Pressure (Pa)	Filter Field (A)	Bias Plate Current (A)
900	3	10	0.01
1000	3	10	0.01
1100	3	10	0.01

From these scans it can be observed that, as expected, the plasma is more ionized at higher RF Power, while the RF Power has not a relevant effect on the electron temperature.

A linear dependence of density with respect to the RF Power was found by performing a scan at fixed position.

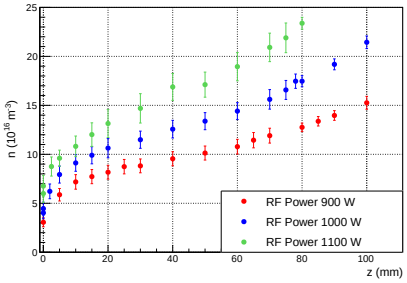

(a) Density along z, different RF power

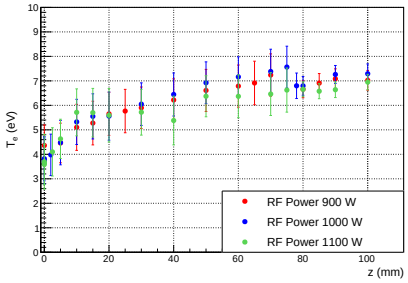

(b) Temperature along z, different RF power

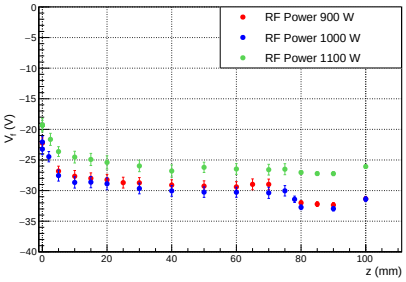

(c) Floating potential along z, different RF power

Figure 3.8

Plasma conditions

Position(mm)	Pressure (Pa)	Filter Field (A)	Bias Plate Current (A)
10 80	2	10	0.01
10 80	2	10	0.01
10 80	2	10	0.01

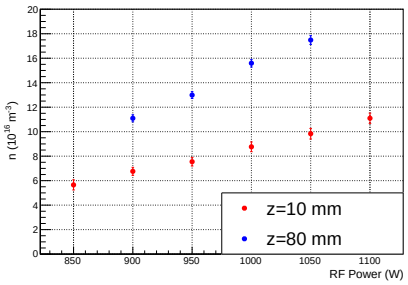

(a) Density at fixed positions, different RF power

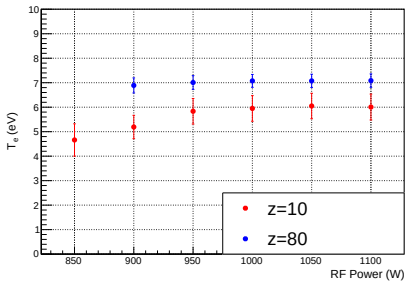

(b) Temperature at fixed positions, different RF power

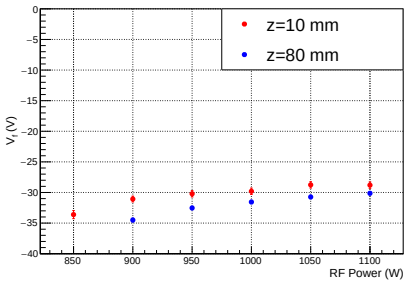

(c) Floating potential at fixed positions, different RF power

Figure 3.9

The linear dependence of density on the RF power is evident in both positions. To quantify this dependence, the angular coefficient of the linear curve that better fit the data is evaluated. From this fit the following parameters, if $y = mx + q$ is the linear curve, are obtained:

- At z=80mm: $q = (-30 \pm 2) \cdot 10^{16} m^{-3}$ and $m = (0.046 \pm 0.002) \cdot 10^{16} m^{-3} \frac{1}{Wm^3}$

- At z=10mm: $q = (-13 \pm 2) \cdot 10^{16} m^{-3}$ and $m = (0.021 \pm 0.002) \cdot 10^{16} m^{-3} \frac{1}{Wm^3}$

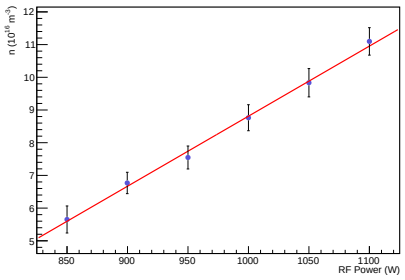

(a) Fit at fixed position 10 mm taking data at figure 3.9 on page 33 $q = (-13 \pm 2) \cdot 10^{16} m^{-3}$ and $m = (0.021 \pm 0.002) \cdot 10^{16} m^{-3} \frac{1}{Wm^3}$

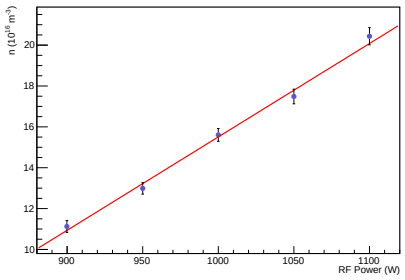

(b) Fit at fixed position 80 mm taking data at figure 3.9 on page 33 $q = (-30 \pm 2) \cdot 10^{16} m^{-3}$ and $m = (0.046 \pm 0.002) \cdot 10^{16} m^{-3} \frac{1}{Wm^3}$

In the same way it is possible to obtain the angular coefficients in different positions of the probe by using the scan performed with the probe along the whole source and with three different values of RF power at figure 3.8 on page 32. For each scan only points at positions 10 mm and 80 mm are considered. From this fit the following parameters, if $y = mx + q$ is the linear curve, are obtained:

- At z=80mm: $q = (-35 \pm 4) \cdot 10^{16} m^{-3}$ and $m = (0.053 \pm 0.004) \cdot 10^{16} \frac{1}{Wm^3}$
- At z=10mm: $q = (-9.35817 \pm 7) \cdot 10^{16} m^{-3}$ and $m = (0.018 \pm 0.007) \cdot 10^{16} \frac{1}{Wm^3}$

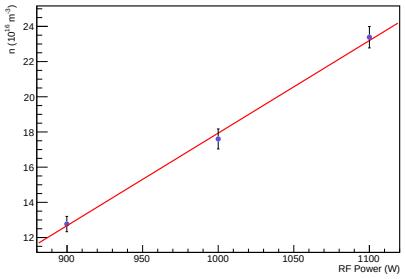

(c) Fit at fixed position 80 mm taking three data at figure 3.8 on page 32 $q = (-35 \pm 4) \cdot 10^{16} m^{-3}$ and $m = (0.053 \pm 0.004) \cdot 10^{16} \frac{1}{Wm^3}$

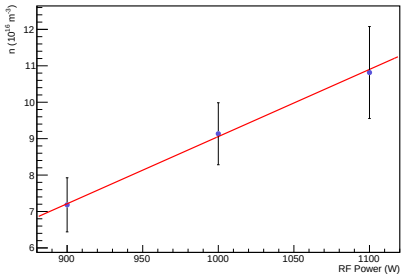

(d) Fit at fixed position 10 mm taking three data at figure 3.8 on page 32 $q = (-9.35817 \pm 7) \cdot 10^{16} m^{-3}$ and $m = (0.018 \pm 0.007) \cdot 10^{16} \frac{1}{Wm^3}$

In the following pictures fig. 3.10 in blu the estimates of the angular coefficients for all the positions of data in figure 3.8 on page 32, in red the estimates coefficients of data at figure 3.9 on page 33 are presented. Even if data taken

from figure 3.9 on page 33 are taken while fixing a different pressure from data in figure 3.8 on page 32, the results are very similar.

The compatibility [12] between the two angular coefficients is calculated and the results are:

- Position 10mm: compatibility between$m = (0.021 \pm 0.002) \cdot 10^{16} m^{-3} \frac{1}{Wm^3}$ and $m = (0.018 \pm 0.007) \cdot 10^{16} \frac{1}{Wm^3}$ is 0.4 which means an optimal compatibility of the two estimates,
- Position 80mm: compatibility between $m = (0.053 \pm 0.004) \cdot 10^{16} \frac{1}{Wm^3}$ and $m = (0.046 \pm 0.002) \cdot 10^{16} m^{-3} \frac{1}{Wm^3}$ is 1.75 which means a good compatibility of the two estimates.

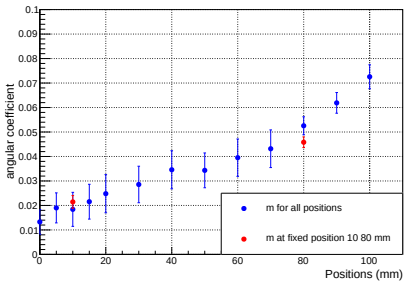

Figure 3.10

3.3.4 BP

Plasma conditions

RF Power(W)	Pressure (Pa)	Magnetic Filter (A)	Bias Plate Current (A)
900	3	10	0.01
900	3	10	0.15

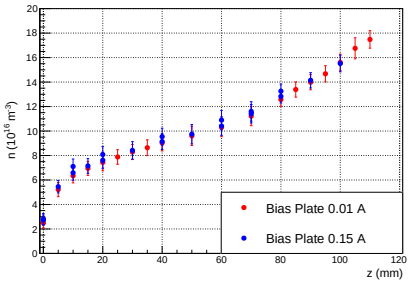

(a) Density along z with and without bias plate current

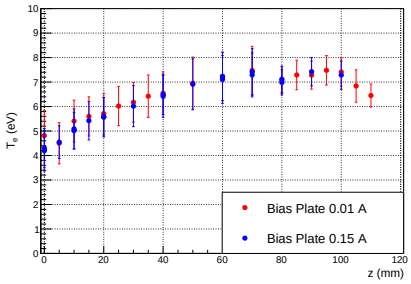

(b) Temperature along z with and without bias plate current

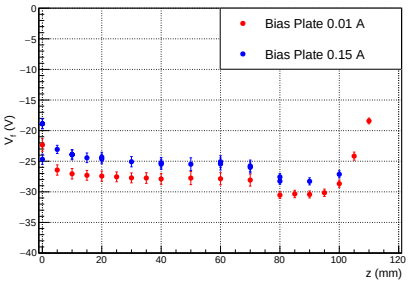

(c) Floating potential along z with and without bias plate current

Increasing the BP polarization, a general decrease of the plasma potential was noticed.

This may suggest that the polarization of the BP implies a changing of the plasma potential in the entire colume of the extraction region.
In order to compare the quantitative variation of the plasma potential in all the positions with the corresponding variation of the BP bias, values of the BP polarization in the two conditions was taken from the datasheet and the plasma potential was calculated from the floating potential with the formula:

$$V_p = V_f + 3.5T_e$$

using as V_f and T_e the values obtained from fit. The resulting graphic presents: in blue the differences between the plasma potential before and red the respective difference of the voltage of the bias plate with and without the bias.

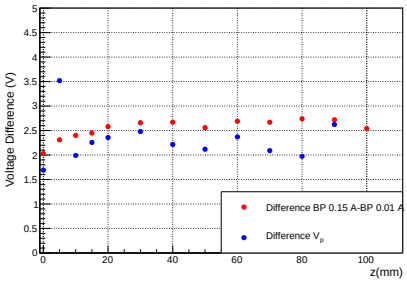

Figure 3.11

Chapter 4

Numerical Simulation of Plasma

A numerical method to simulate plasma inside the NIO1 source had already been developed in another work, in order to study the electron transport across the magnetic filter[15]. In this chapter the main characteristics of the code are presented and it is explained how it was used to reproduce some of the conditionsinvestigated during the experiments reported in this thesis.

4.1 Particle in Cell Method

Particle in Cell (PIC) is a numerical method based on the calculation of the trajectory of a great number of particles inside a domain.
The model consists of charged particles moving inside the chamber due to the forces of their own field. The number of particles is not the real one, but essential physics can be captured with a much smaller number of particles than that in a real plasma, by condensating the behaviour of several particles in the so called macroparticles. Upon calling q the charge of a particle (such as the electron charge) and m its mass, a macro-particle is constituded by several particles (10^6 - 10^8), while preserving the ratio $\frac{q}{m}$ in order not to change the parameters of the equations of motion of the particles.

The study of the evolution of the system is discretized in time step, inside which many numerical processes are performed to simulate particle movement and fields changes, because one implies the other. The space of the chamber in which particles move is also discretized: it is subdivided into cells forming a grid, whose extremes are called nodes.

The main steps of the numerical process are summarized in 4.1:

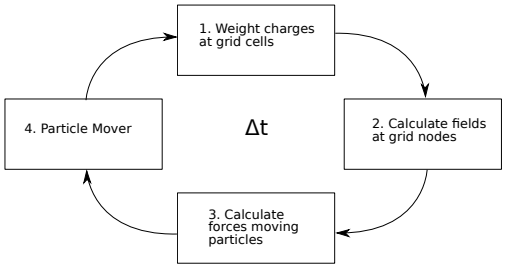

Figure 4.1

The method follows an iterative approach: at each iteration all the steps mentioned in 4.1 are realized. In the following, the steps of the process numbered in the previous scheme are described more in detail:

At the start of the code particles are generated uniformly in all the domain. Each particle is characterized by its charge and mass and occupies a position into the chamber and possesses a temperature and a velocity.

1. the charge of the particles contained into a cell is deposited at its extremities and from that it is possible to calculate the charge density at each node. An example of charge deposition in one-dimensional case (this is the simplest case, but in general it can be implemented and realized in 2D or 3D) is reported in 4.2:

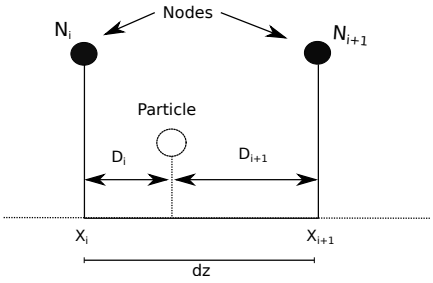

Figure 4.2: Example of deposition of charge at the nodes of the cells which extends from X_i and X_{i+1}. D_i and D_{i+1} are the distances of the particle from the nodes N_i and N_{i+1}. Taking $X_{i+1} - X_i = 1$ and Q the particle charge, in this case the particle charge is divided by weighting it on the distances. At node N_i a portion of the charge QD_{i+1} is deposited, and at node N_{i+1} the deposited charge is QD_i.

2. The Poisson equation is solved to compute the electrostatic fields at the nodes by using the quantities deposited on the nodes according to the procedure described in the previous step.

3. Upon knowing the values of fields at the nodes, and the positions of particles, the forces acting on particles can be calculated. Fields are calculated exactly at each particle position, using an interpolation from the values of the potential, by solving the Poisson equation evaluated at the nodes at the previous step.

4. Particles are moved: the scheme used to integrate the Lorentz force law, is that of the Boris method[13].

The scheme described is iterated over a fixed number of steps, usually until the system reaches a certain equilibrium on a stable condition.

4.2 1D3V PIC-MCC Method

The PIC method used is called 1D-3V. 3V means that positions and velocity of N particles are tracked in 3D cartesian coordinates and the velocitis in all three directions are considered; equations of motions for particles are then calculated in three dimensions, but at the same time the charge of particles is deposited on a 1D grid, and the Poisson equation and fields are calculated only along one single direction, that in our case is the beam direction z, which is the same direction in which the probe has been moved during the diagnostic operations. The model domain is the entire NIO plasma chamber, whose dimensions in the code represent the real dimension of the NIO source.

Some important differences with the real condiiton have to be mentioned:

- In the driver region, the RF plasma coupling has not been modeled yet, but the heating and refueling of plasma is taken into account by re-sampling the energy of a certain number of particles at each time step according to a Maxwellian distribution at a given temperature which is a user input. This fixes the average temperature of the electron in the region corresponding to our driver and the code only calculates the behaviour of plasma density and temperature outside this region. The validity of this method to approximate a uniform source of hot electrons was proposed in [14]

- The model only takes into account two species: electron and positive ions while negative ions (that are present in reality in the NIO source) are neglected. This choice is anyway acceptable because, as explained in 1.1, in the absence of caesium vapor, negative ions represent everywhere only a fraction of the negative ion charge.

As the code starts running, random variables are generated to determine the position and velocity of each particle and energy is calculated.

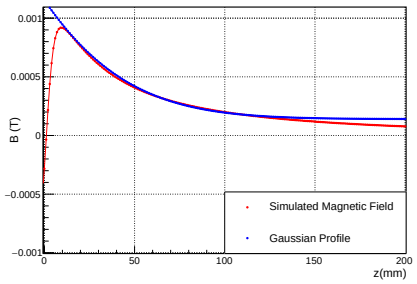

Figure 4.3: Comparison between the simulated profile using OPERA-TOSCA code (this study is taken from [15])of the magnetic filter and the gaussian profile used in the code

Two simulation grids are generated, one for electrons and one for ions, to deposit the respective charge density at the nodes. The sum of the charge densities is then stored in a third grid, which is used to calculate the local electric field and potential by integrating the Poisson equation. The radial contribution on electric field is taken in account by introducing an artificial electric field: starting from the potential calculated by the PIC at the centre of the chamber and going to the walls, the drop of potential is expected to be moderate inside the bulk of plasma, but significant in the plasma sheath, that forms the plasma-wall transition.

After that particle are moved, a check if their position is inside the limits of the chamber is made. If an electron is found outside of the chamber region, the particle is simply deleted. If an ion is founded to be outside the chamber, an electon-ion pair is introduced in the driver region, at the following iteration, so that the number of ions is constant during the simulation[16].

The magnetic field is modeled by assuming a simplified gaussian profile,4.3 which is a good approximation of the B field shape before the PG as reported in fig. 4.8 This had been made by the author of the code with the aim of simulating the magnetic filter in NIO 1.1.

Apart from the few mm in the proximity of the plasma grid, this is a good approximation of the real field.

Even if the presence of neutral gas is negligible in the calculation of potential, ion and electron density ,it has a major effect in collisions of electrons. To account for the presence of gas in the code, the PIC method is coupled with MCC (Monte Carlo Collisions technique), a simple method for modeling particle collisions, in which the neutral gas density is included in the code as a fixed background to take account of elastic and ionizing collisions of electrons with neutrals in addition to Coulomb collisions of electrons with ions.
At each iteration, the energy possesed by the electrons can be calculated, and for each range of energy the particle will have a different cross section. [18] [19]

Following the MCC method, for each particle and each kind of collision, the collision probability can be calculated as $P = 1 - exp(\sigma n v dt)$, where v is the velocity of the particles, σ is the cross section, n is the gas or the ions density and it is then compared to a random number. If the probability is larger than the random number, the collision occurs and a process-specific collision handler is called. After the collision the velocity of particle is adjusted depending on the collisional event.

4.3 Simulation Results

There are several parameters, in the code, that can be changed to simulate plasma. The aim of the work done in this part of the thesis is to obtain some results with which compare the experimental results. The input parameters that were changed, then, were the pressure of the neutral gas and the intensity of the magnetic filter, as the RF coupling is not modeled in the code. The main results of the code are particle density and temperature, and electrostatic potential. The densities of ions and electrons, as well as the potential, are calculated directly by the code at each iteration, while the particle temperature is calculated using the average temperature of the particles in each cell of the discrete grid.

All these simulations were made with an initial density of particle 10^{15} even if from measurements we well know that density is at least two orders of magnitude higher.
This choice is motivated by the fact that in PIC simulation the required number of cells is not arbitrarily fixed, but must fulfill the criterion dz$<\lambda_D$ where dz is the cell lenght and λ_D is the Debye lenght defined in equation 2.1. This means that simulations made at high densities require a higher number of nodes to be solved and consequently, to assure a suitable population of particles in each cell of the domain, a higher number of particles are required and have to be moved. In order to reduce the computational cost of high density simulations (tens of days, by using a standard processor), a scaling procedure is adopted, as suggested in [14].

In order to validate the scaling procedure proposed by [14], a set of simulations at different densities was performed, by simulating the plasma in a chamber five times smaller than the real one.
The results are reported in figure 4.4.

If in the driver, the trends of electron density and temperature and the electrostatic potential are very similar, their behaviour changes a lot while approaching the wall.

It is well known that if inside the chamber the quasi-neutrality of plasma is verified (ions and electron densities is the same), near the wall of the chamber there is a small sheath (whose lenght is 10-15 times the Debye length) in which ion density is higher than electron density.
Because of the fact that λ_D is inversely proportional to the square root of the density, this sheath length will be different in simulations with different densities.

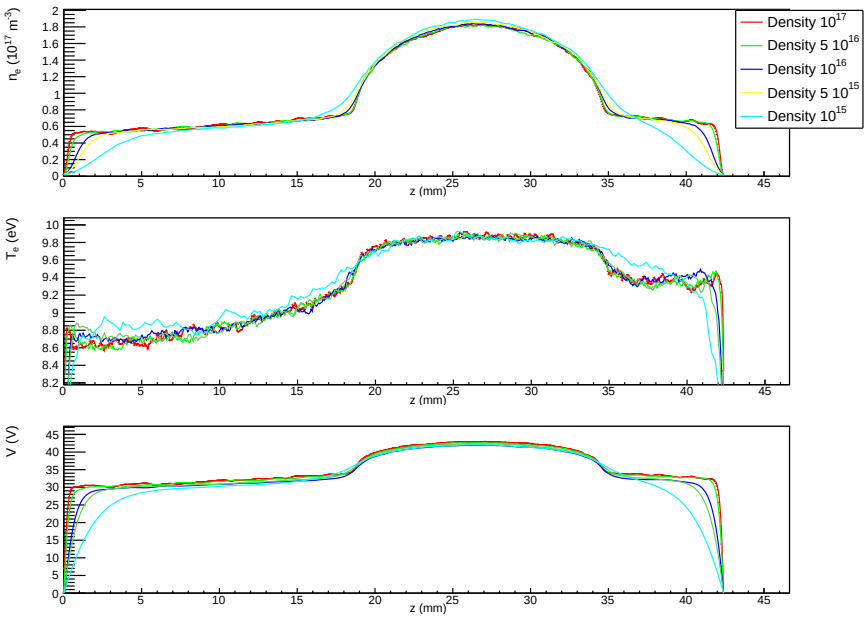

Figure 4.4: Review of simulations results. Density profiles are scaled, in order to be compared

The sheath can be seen by plotting in the same graphic the ion and the electron densities: in figure 4.5, as an example, the results on ion and electron density in the simulation with initial value of density 10^{16} are reported.

In the top picture the entire profile of density in the chamber is reported, while in the bottom picture, the attention is focused on the first millimeters of the curve, where the sheath is present.

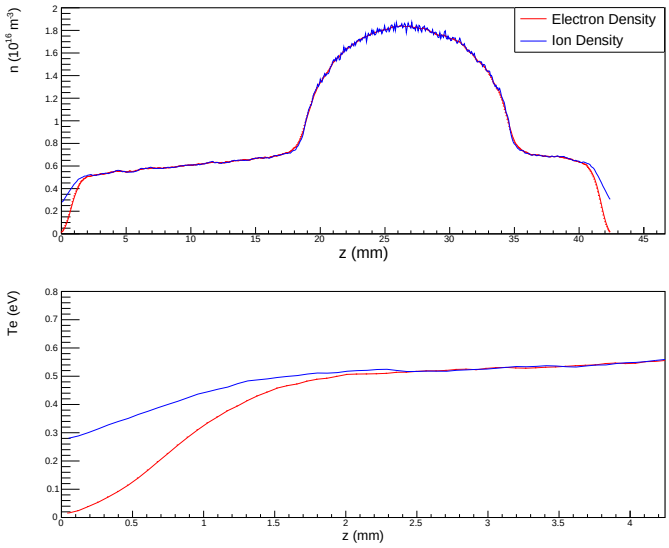

Figure 4.5

The sheath length for each value of density were then evaluated and their estimates are compared. The sheath length was extracted by searching for a point of the chamber in which ion and electron density profiles could be considered enough separated. A method which could give a good estimate of the sheat lenght was to search the position in the chamber, in which the ion density was found to be 1.025 times the electron density. For lower or higher coefficients, the estimate was not precise. This was made by using a MATLAB program. As an example, in the simulation presented in 4.6, the sheath lenght founded by the code, is $2mm$.

The results are presented in figure 4.6: The black line represents the trend of a theorical sheath with a length equal to 10 times the Debye length. In this case, the Debye length is calculated taking T_e=8.7 eV, which is almost the temperature reached by the simulated plasma in position $z = 10$ (fig 4.4).

The case in which the sheat length is bigger is that in which the initial density is 10^{15} $\frac{particles}{m^3}$.
If the sheat length is extimated to be 10 times the Debye length (and in this case $\lambda_D = 0,743mm$), it means that it extends inside the chamber for at least $7,43mm$ at both side of the chamber.
Then, in this case, in which the chamber length is set to be $42.4mm$, the sheat lenght cannot be neglected.

In the simulations used to compare with the experimental data, instead, the chamber length is set to be $21cm$ long, according to the real dimensions of the chamber. The initial density is 10^{15} $\frac{particles}{m^3}$, so the sheath length, this time, is much smaller with respect to the chamber. Then the choice of comparing

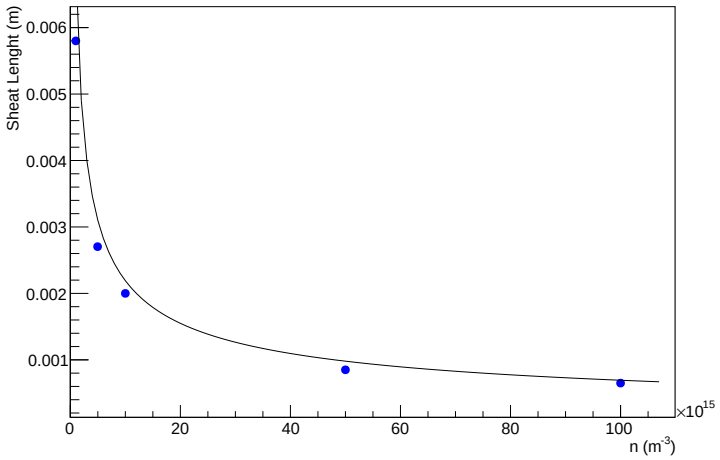

Figure 4.6: In blu, the sheath length estimated by simulations, in black is tracked the curve of the sheath lenght (taken as ten times the Debye length) as a function

experimental data with simulations with a lower density than 10^{17} $\frac{particles}{m^3}$, is well justified, but points near the walls are less reliable.

4.4 Comparison between simulations and experimental data

As verified in the previous section 4.3 a simulation with initial density of 10^{17} $\frac{particles}{m^3}$ would give qualitatively the same profile for electron temperature and density as that with initial density of 10^{15} $\frac{particles}{m^3}$ (the only exception are points near the walls, but it is good to remember that they were not taken in account also in experimental results 3.3).
Then, even if the density in the simulation and that measured by the probe inside the NIO1 chamber are very different, the results can be compared anyway by normalizing the data. The choices made for the normalization of data in the following results , will be explained case by case.
Temperatures, instead, can be compared without normalization. The results obtained with the experiment by changing the magnetic filter intensity are then reproduced using the PIC code.
In the code, this can be made by changing the parameters of the gaussian whose shape reproduces the intensity of the magnetic field present in the extraction area when, in the real case,the magnetic filter activated. As already explained in 1.1, in NIO1 the magnetic field intensity is controlled by means of the current flowing trought the PG.

Because of the fact that, in the code, the gaussian trend of the magnetic field was built so as to reproduce the field generated for each value of current set during experiments, the simulation results are presented referred to the current value.

4.4.1 Comparison of scan in position

In order to compare numerical and experimental scans in position with fixed external condition, data are normalized at the value of density at position z=20mm, as it can be observed in Figure 4.7 This choice was made because, as explained, points near $z = 0$ must be neglected.

Here experimental data in density and temperature for a scan at fixed position in condition of gas pressure at 6 Pa (3.4) with minimum and maximum values of the magnetic filter current are compared to the simulation results. In both cases density and temperature are normalized in the following way:

- in case of minimum value of the magnetic filter current (10 A), the values of density at the position of $z = 20mm$ are, for experimental data $8.8 \cdot 10^{16}$ $\frac{particles}{m^3}$ and for simulated data $0.2 \cdot 10^{15}$ $\frac{particles}{m^3}$
- in case of maximum value of the magnetic filter current (400 A), the values of density at the position of $z = 20mm$ are, for experimental data $9.7 \cdot 10^{16}$ $\frac{particles}{m^3}$ and for simulated data $0.2 \cdot 10^{15}$ $\frac{particles}{m^3}$

It must be observed that, because of the fact that during the diagnotic experiments only the first 100-110 mm of the chamber was studied, but above 90mm perturbation of the plasma occurred so that the first part of the simulated curve is presented. The electron density and temperature obtained with experimental data are well simulated by the code.

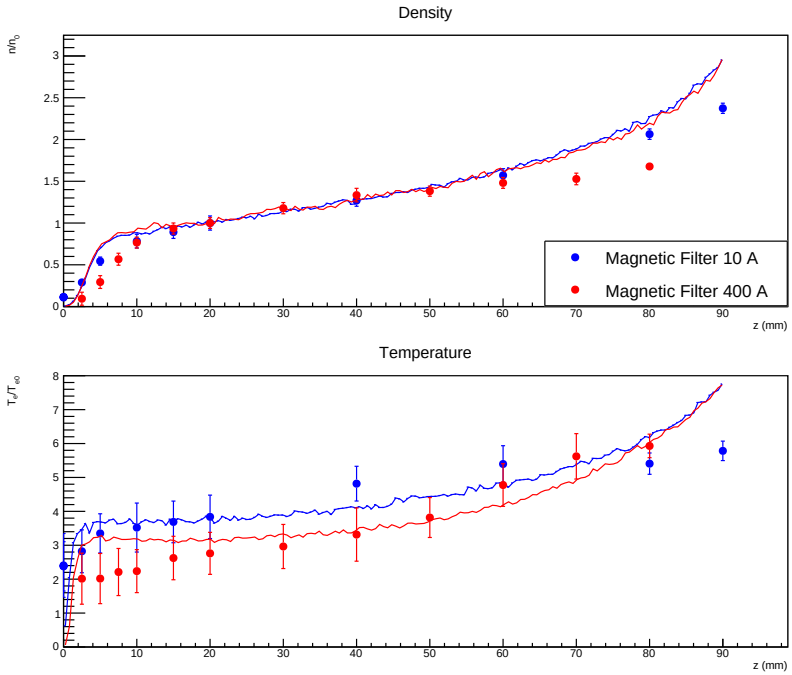

Figure 4.7: Comparison between experimental data (red dots) and simulation (blue line)

In the presence of the magnetic field the data analysis shows a decrease of the electronic temperature as its intensity is higher. In the following picture4.8,the results of the simulation for the electron density and temperature, at different values of the magnetic filter current are presented.

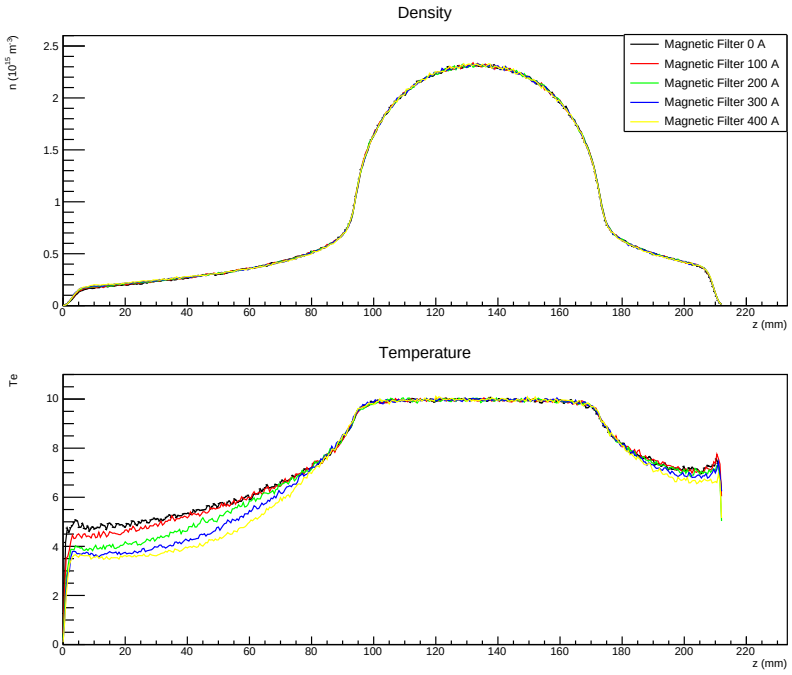

(a)

Figure 4.8

The effect of the magnetic filter on temperature can be observed: the electron temperature is lower for higher simulated magnetic filter. On the other hand, the difference between the density profiles is negligible.

It can be interesting to compare the scan in magnetic filter, obtained while keeping the probe at fixed positions (3.3) with simulation results. For each trend in 4.8 the data with position $20mm$ were selected, and were compared to the experimental results .

To compare data with different magnetic filter but same position, densities are then normalized at the first value of B scanned.

Both in simulations and in experimental results, the temperature decreases with almost the same trend.

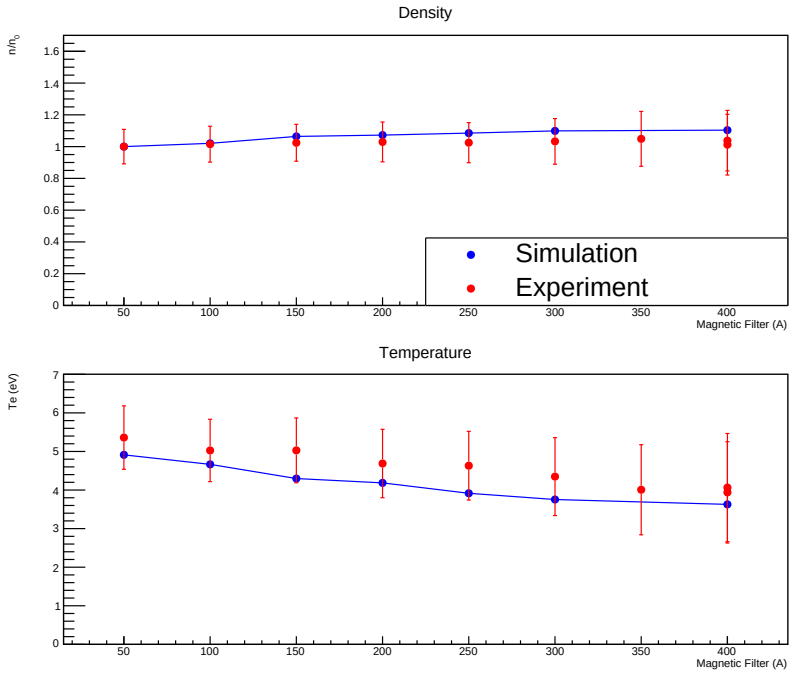

(a)

Figure 4.9: Scan of magnetic field at fixed position 20mm. Data in density were normalized at the first value of density at 20 mm(current of the magnetic filter at 50 A): $8.3 \cdot 10^{16}$ for experimental data, $0.3 \cdot 10^{15}$ for simulated data

The last aspect that is investigated is the effect of pressure on electron temperature and density.

At the beginning of the code it is possible to set the pressure of the neutral gas, so several simulations at different pressure are made. Then, by taking the values of density and temperature in position 10mm, the resulting values can be compared to the experimental data presented in 3.5.

The experimental data in 3.5 are acquired by keeping the probe at the fixed position of 10 mm while varying the pressure of the neutral gas.

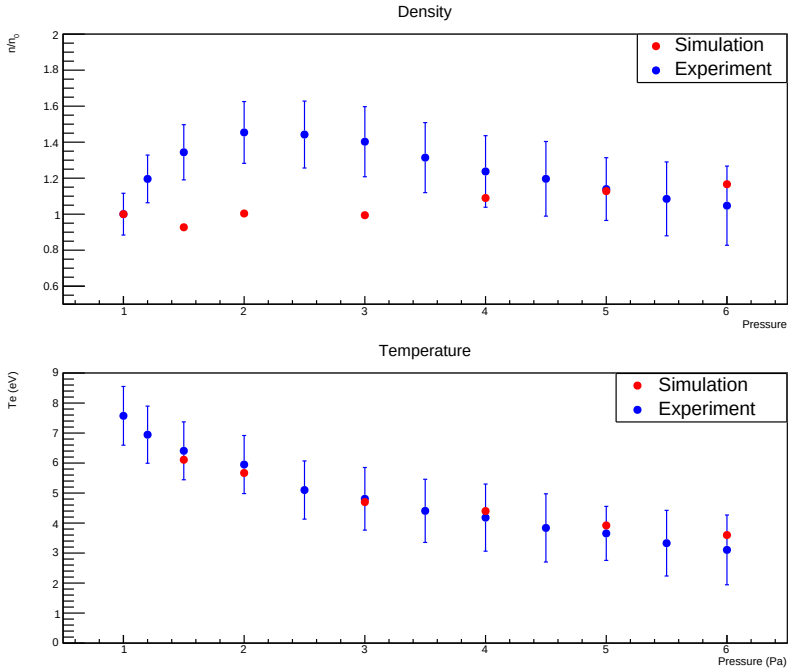

Figure 4.10: Scan of pressure at position 10mm. Data in density were nomalized at the first value of density at position 10mm (pressure of 1Pa): $8.4{\cdot}10^{16}\ \frac{particles}{m^3}$ for experimental data, $0.2 \cdot 10^{15}\ \frac{particles}{m^3}$ for simulated data

Also in simulations, the decrease of temperature as the pressure rises can be observed. And experimental data well agree with the simulation results. It can be observed, however, that a maximum in density is presented in the experimental data, but not in the simulation. The presence of the maximum, can be due to the the coupling of plasma with the RF power, an aspect that is not simulated in the PIC code.

Chapter 5

Conclusions

In this work the diagnostic setup used to investigate the plasma properties inside the negative ion source NIO1, consists of a Langmuir probe,essentially made of a biased electrode, inserted into the plasma. By analyzing the particles flux collected by the probe, the main plasma parameters (the electron density and temperature) and the floating potential of the probe, were deduced in the entire extraction area of the source.

A particular attention was paid to the study of electron density and temperature variations. During the campaign of measurements the conditions of pressure, applied power and magnetic field intensity were changed.
Measurements were acquired at different values of the magnetic field in the extraction area and at different values of pressure of the neutral gas and of the RF power, and scans both at fixed positions of the probe and by moving the probe along the axial direction of the source were performed. Analysis of the measured data allowed to verify some important aspects: the NIO1 magnetic filter has a cooling effect on electron temperature, which is more evident in cases with low pressure of the neutral gas (3 Pa or 1.5 Pa), while it is less evident for higher pressures.
Also the pressure has a cooling effect on the electrons, as a consequence of the increased collisionality of electrons with the neutral gas. A maximum value of the density of the plasma near the plasma grid was found for a value of pressure of 2 Pa. The linear increment of the electron density as the RF Power was increased, that is expected by the theory, was also verified.

In order to numerically investigate and interpret the experimental results, a code based on the PIC method was used. The adaptation of the code, to describe the plasma of NIO required a scaling procedure to have a reasonable computational load. The consistence of the scaling procedure was validated and the sheat thickness in proximity of the walls was verified to be few times the Debye length, as according to the theory.

The experimental data resulted in general in good agreement with the simulation: in particular, in the pressure scan with the probe at fixed position, the temperature present almost the same profile in the two cases both qualitatively

and quantitively. In the pressure scan at fixed position, instead, the maximum in ionization for density was not evident in the simulation, but this effect can be explained by the fact that in this case the RF coupling with plasma was not modelized. In the scan of the magnetic field with the probe at fixed position, instead, both temperature and density obtained from the data analysis exhibit almost the same profile as those obtained by the simulations.
A deeper analysis of the experimental results can be an interesting theme for future studies. In most of the cases, the study of the profiles of electron temperature and density and of the gradient of the plasma potential might give information on the presence of diffusive phenomena and/or electric fields inside the plasma.

These measurements of the electron temperature in the presence of the magnetic filter have confirmed the fact that electron temperature in the extraction region of the NIO1 source is high in comparison to other ion sorces, and in order to optimize the future negative ion extraction, the strength of the magnetic field used for the electron cooling must be increased. Indeed, using permanents magnets, the increase of the magnetic field has already been carried out, but the investigation of the source features by Langmuir probe has not been possible as yet. More generally, when the source parameters and particularly the RF power, will be raised to nominal parameters, a new characterization of NIO1 cource will be necessary.

A lot of work can be made also in the upgrade of the PIC numerical code introducing a model for the RF plasma coupling and the introduction of other charged species of particles that at present are not included in it, but in reality are present in the plasma, like H_2^+,H_3^+,H_-.

Bibliography

[1] M. Kikuchi, K. Lackner, and M. Tran, Fusion Physics. IAEA: International Atomic Energy Agency,2012.

[2] E. Speth et al. *Overview of the RF source development programme at IPP Garching*, Nucl. Fusion 46, S220 (2006)

[3] M. Bacal, M. Wada, *Negative Hydrogen ion production mechanism* Applied Physics Reviews 2, 021305 (2015)

[4] ITER "www.iter.org/"

[5] I. Brown, *The Physics and Techology of Ion Sources*, Wiley-VCH, 2nd ed., 2004

[6] R.S. Hemsworth and T. Inoue,*Positive and Negative Ion Sources for Magnetic Fusion*, IEEE Transactions on Plasma Science, p.1800 (2005)

[7] M. Cavenago, T. Kulevoy, S. Petrenko, G. Serianni , V. Antoni , M. Bigi ,F. Fellin ,M. Recchia ,P. Veltri *Development of the versatile multiaperture Negative Ion source*, Rev Sci Instrument vol. 83,no.2,2012

[8] M. Liebermann and A. Lichtengerg, *Principles of plasma discharge and material*, Wiley - Interscience, 2 ed., 2005

[9] M. Cazzador *Analytical and numerical models and first operations on the negative ion source Nio1*, Matster's thesis, University of Padua, Dept. of Physics and Astronomy, 2014

[10] I. H. Hutchinson, *Principles of Plasma Diagnostic*, Cambridge university press, 2002

[11] D. Desideri and G. Serianni, *Four parameters data fit for Langmuir probes with non saturation of ion current*, Rev Sci Instrument vol. 69,2354, (1998)

[12] M. Loreti *Teoria degli errori e Fondamenti di Statistica*, Edizione privata fuori commercio, 2006

[13] J. Boris. *Proceeding of Fourth Conference on Numerical Simulations of Plasmas* (Naval Research Laboratory, Washington D.C., 1970)

[14] J.P. Boeuf, B. Chaudhury and L.Garrigues *Physics of a magnetic filter for negative ion sources. I. Collisional transport across the filter in an ideal, 1D filter*, Physics of plasma 19,113509(2012)

[15] P. Veltri, E. Sartori, M. Barbisan, M. Cavenago, G. Serianni and B. Zaniol *Study of electron transport across the magnetic filter of NIO1 Negative Ion Source* 2016

[16] L. Garrigues, G. Fubiani and J. P. Boeuf *Negative Ion extraction via particle simulation for fusion: critical assesment of recent contributions*

[17] G. Serianni et al. *Acquisition, Data Retrieval, Interlock and Control System for the Negative Ion Source NIO1*, AIP Conf. Proc.

[18] J. Yoon, M. Song, J. Han S. Hwang, W. Chang B. Lee and Y. Itikawa *Cross sections for electrons collisions with Hydrogen Molecules* Journal of Physical and Chemical Reference Data 37, 2008 p.918

[19] R. K. Janev, W. D. Langer, K.Evans Jr. and Douglass E. Post Jr *Elementary Processes in Hydrogen-Helium Plasmas*, 1987 p.34-54,172

[20] M. Cazzador et al.*Semi-analytical modeling of the NIO1 source* AIP Conf. Proc. 1655, 020014, (2015)

Appendix

Magnetic Filter

Plasma conditions

RF Power	Pressure (Pa)	Filter Field (A)	Bias Plate Current (A)
900	3	10	0.01
900	3	400	0.01

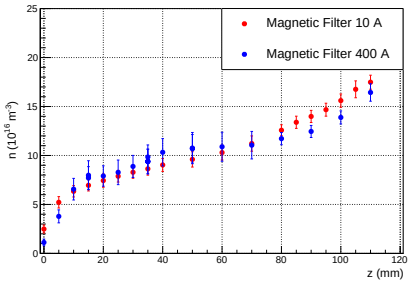

(a) n along z, magnetic filter at 10 and 400 A

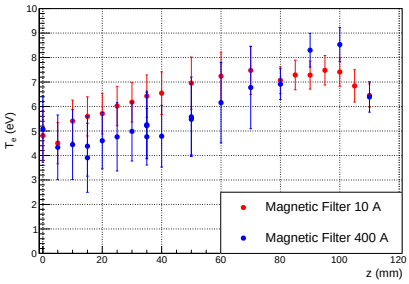

(b) T_e along z, magnetic filter at 10 and 400 A

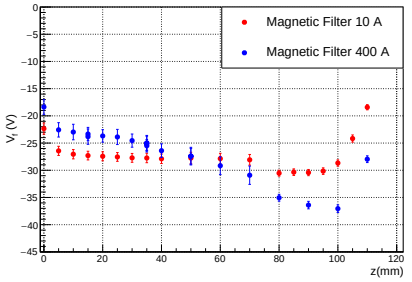

(c) V_f along z, magnetic filter at 10 and 400 A

Comparison between the direct measurement of floating voltage and the fit results.

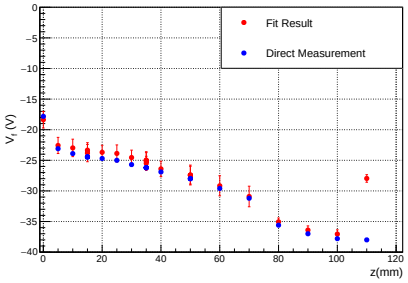

(a) Comparison between the direct measurements of floating voltage and the fit results with magnetic filter at 400 A

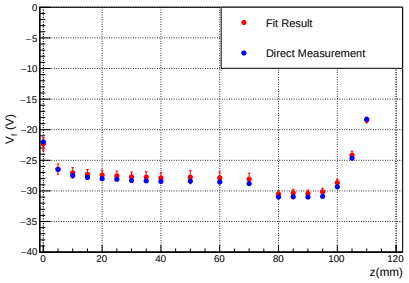

(b) Comparison between the direct measurements of floating voltage and the fit results with magnetic filter at 10 A

Plasma conditions

RF Power	Pressure (Pa)	Magnetic Filter (A)	Bias Plate Current (A)
1100	2	10	0.01
1100	2	400	0.01

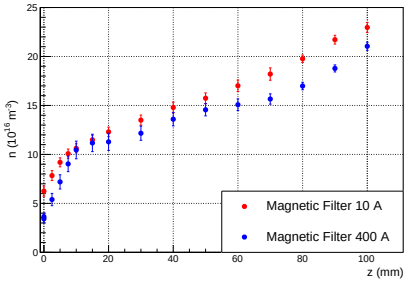

(a) n along z, magnetic filter at 10 and 400 A

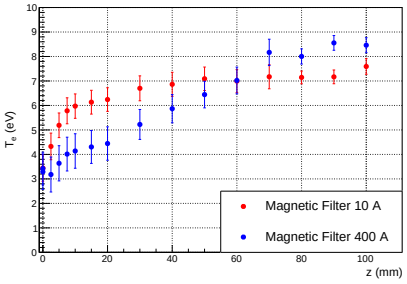

(b) T_e along z, magnetic filter at 10 and 400 A

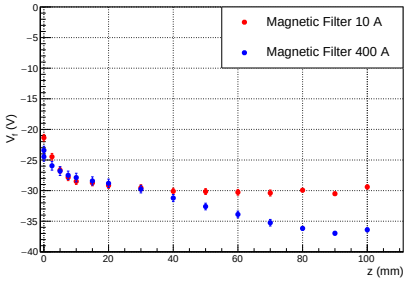

(c) V_f along z, magnetic filter at 10 and 400 A

Figure 1

Plasma conditions

RF Power	Pressure (Pa)	Position (mm)	Bias Plate Current (A)
1100	3	10	0.01

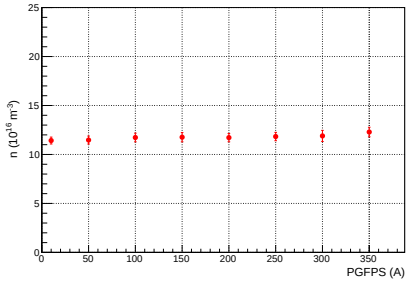

(a) Density at z=10 as a function of magnetic filter

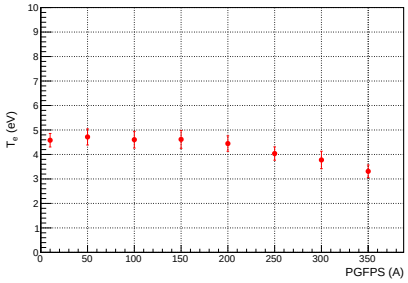

(b) Temperature at z=10 as a function of magnetic filter

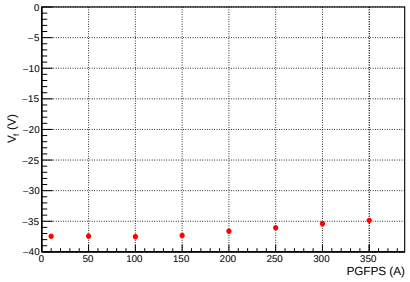

(c) Floating potential at z=10 as a function of magnetic filter

Pressure

Plasma conditions

RF Power (W)	Pressure (Pa)	Filter Field (A)	Bias Plate (A)
900	1.5	10	0.01
900	3	10	0.01
900	5	10	0.01

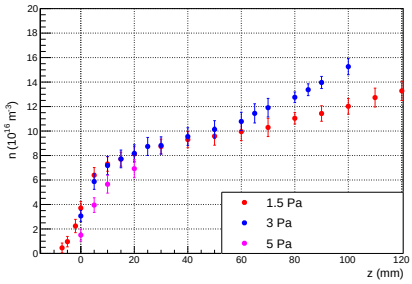

(a) Density along z with different values of pressure

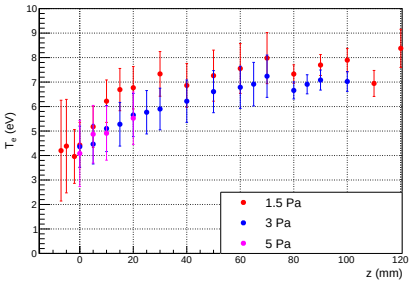

(b) Temperature along z with different values of pressure

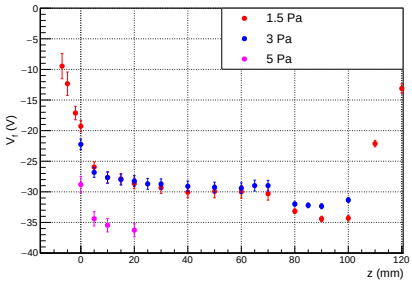

(c) Floating potential along z with different values of pressure